Chapter VI

Structure, Surface Morphology and Magnetic Properties of 900 ºC Annealed TiO_2 Thin Films under Ar^{2+} Ion Irradiation

6.1 Introduction

In the previous chapter, we have demonstrated the effect of 500 keV Ar^{2+} ion irradiation on structural and magnetic properties of TiO_2 thin films deposited through e-beam evaporation technique and annealed in oxygen environment at 500 ºC. The present chapter describes the creation of post-deposition defects by Low Energy Ions (LEI) and its effect on structural and magnetic behaviour of TiO_2 thin films annealed at 900 ºC. The pristine film annealed at 900 ºC for 1 h (deposited on Si), films irradiated with ion fluence 1 × 10^{14} and 5 × 10^{16} ions/cm^2 referred as A, B and C respectively. Structure and surface morphology of these films are elaborated in section 6.2. Magnetic properties are discussed in section 6.3. Section 6.4 describes X-ray photoelectron spectra of the samples. Section 6.5 summarizes the experimental findings.

6.2 Structure and Surface Morphology

In this section, we have presented structural and surface morphology studies carried out by X-Ray Diffraction (XRD), Raman Spectroscopy, Rutherfoed's Back Scattering (RBS) and Atomic Force Microscopy (AFM).

6.2.1 Rutherford's Backscattering

Figure 6.1 depicts the RBS spectra of pristine film (A), film irradiated with an intermediate fluence of 1 × 10^{14} ions/cm^2 (B) and the film irradiated with ion fluence 5 ×

10^{16} ions/cm^2 (C). Element that has been detected from the RBS measurement are Ti, Si and O. The width of the Ti curve, before and after ion irradiation is almost same, which indicates

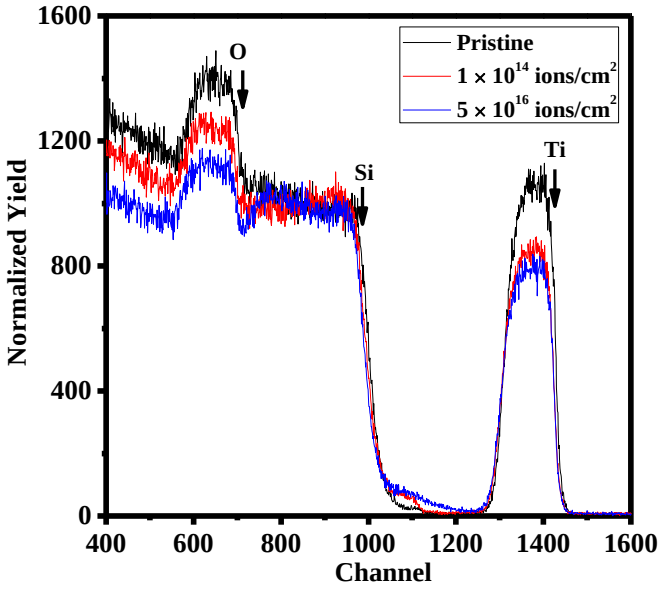

Figure 6.1 *RBS spectra of TiO_2 thin films indicating Ti, Si and O edges.*

that thickness of pristine and irradiated films are almost same. As R_p (363 nm) is higher than the film thickness (~300 nm), the projectile ion gets implanted deep inside the substrate.

6.2.2 X-Ray Diffraction and Raman Spectroscopy

Figure 6.2 depicts the glancing angle X-ray diffraction (GAXRD) patterns of film A, B and C. The most intense peak observed at 25.35º in film A, B and C either corresponds to (101) of anatase phase of TiO_2 (JCPDS PDF# 894921) or (120) of brookite phase TiO_2 (JCPDS PDF# 761934). However, it is observed that the intensity of the peak at 25.35º increases in film C followed by a significant decrease in intensity observed in film B. It shows that all the films are crystalline in nature but in film B as the peak intensity decreases

that shows film tends to amorphisation after irradiation, same as in film annealed at 500 ºC. Besides the peak at 25.35º, six more peaks observed at 23.73º, 26.53º, 27.53º, 29.3º, 34.96º and 37.83º, corresponds to the Magneli phase (Ti_4O_7) in film A, B and C (JCPDS PDF# 771392). The intensity of the above peak does not show any change with fluence. Thus, Ti_4O_7 phase shows radiation resistance behavior. Previously, Ti_4O_7 phase has not been observed by us in TiO_2 thin films annealed at 500 ºC in oxygen environment before or after irradiating with 500 keV Ar^{2+} ions. The appearance of Ti_4O_7 phase observed here would be due to increasing annealing temperature. Due to noise in the XRD pattern, we have carried out Raman measurement to confirm the phase. Figure 6.3 show the Raman spectra of the films A, B and C. Film A and B, show peaks at 144, 396 and 637 cm^{-1}, which corresponds to E_g, B_{1g} and E_g modes of anatase phase [Ricci et al. (2013)]. Film C shows peaks at 151 cm^{-1} and 634 cm^{-1} which correspond to A_{1g} mode of brookite phase only. A similar appearance of Raman peaks are reported for brookite phase of TiO_2 by Iliev et al. (2013). Combining XRD and Raman results, we observe a transformation from anatase to brookite phase after irradiating with 500 keV Ar^{2+} ion of fluence 5×10^{16} ions/cm^2. Suppression of peak at 521 cm^{-1} related to Si substrate observed in the Raman spectrum with ion fluence which indicates creation of defect in silicon substrate after irradiation. Thus, low energy ion irradiation, not only induces a phase transformation from anatase to brookite phase in TiO_2 thin film, it also damages the silicon substrate beneath the film, because the projected range (R_p) of the irradiated ion is higher than the thickness of the film. Among three existing phases of TiO_2 such as rutile, anatase and brookite, it may be mentioned that while anatase and rutile are most commonly occurring phases of TiO_2, whereas brookite phase is rarely observed in TiO_2. Previously, Rath et al. (2009)b observed transformation of anatase to

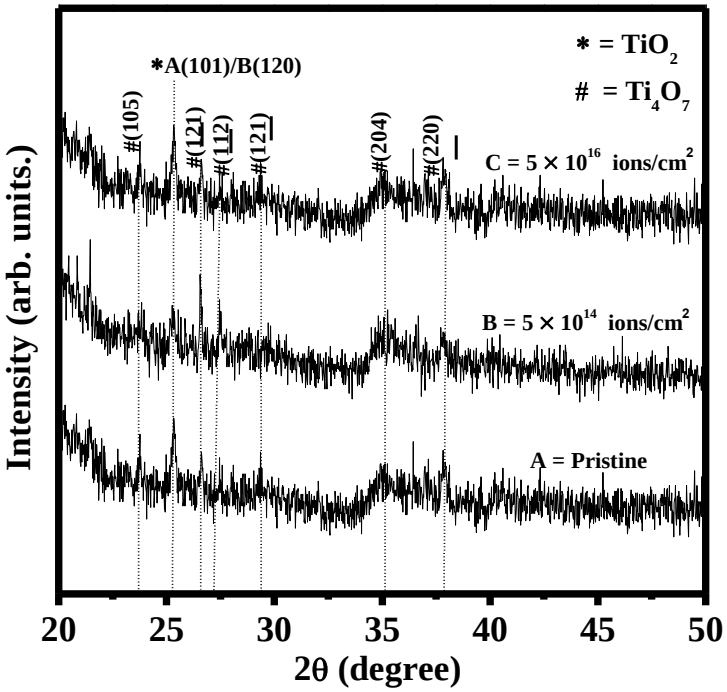

Figure 6.2 *GAXRD pattern of TiO_2 thin films annealed in O_2 environment at 900 ºC before and after irradiation with 500 keV Ar^{2+} ions.*

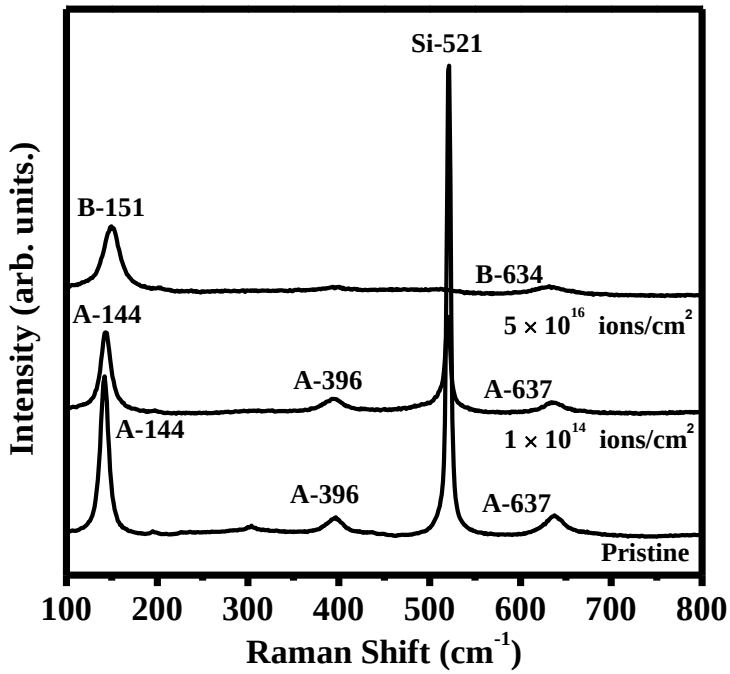

Figure 6.3 *Raman spectra of TiO_2 thin films annealed in O_2 environment at 900 ºC before and after irradiation with 500 keV Ar^{2+} ions.*

rutile phase in TiO_2 thin films after irradiation with 200 MeV Ag ions. With the same ion, but with film of different microstructure, Thakur et al. (2011)b, reported a phase transformation from anatase to mixed rutile and brookite phases. Mohanty et al. (2014)b show amorphisation after irradiating with 100 MeV Ag ion beam. All the stated studies involved swift heavy ions. On the contrary, the present study shows a transformation from anatase to brookite phase of TiO_2 under low energy ions (500 keV Ar^{2+} ions), where S_n induced processes play a dominant role. In addition Ti_4O_7 phase, anatase to stable brookite phase transformation observed first time in TiO_2 thin films by ion irradiation in this case.

6.2.3 Atomic Force Microscopy

We have studied the surface morphology the films through roughness and grain structure analysis. Figure 6.4 (a), (b), (c) depict the surface topography of the film A, B and C, respectively. Figure 6.4 (d) to (f) show the 3D representation of the aforementioned film surface topography. In all the figures, scan surfaces with evaluation area is 1 μm × 1 μm. Topography of the films indicates non-uniform surface. Nevertheless, from 3D representation, one may note that all the films having nano-hillock like structure with variable sizes are distributed unevenly over the film surface with incongruent texture. The surface roughness can be quantitatively expressed by the root mean square roughness (R_{rms}). The R_{rms} is defined as the root- mean square average of height deviation taken from the mean data and expressed as [Mohanty et al. (2014)a]:

$$(\Sigma z_i^2/n = R_{rms})^{1/2} \ldots\ldots\ldots\ldots\ldots\ldots (6.1)$$

where, z_i is height at i^{th} position of the tip and n is the number of data points. R_{rms} is found to be 0.077, 0.065 and 0.063 nm for film A, B and C respectively. The reduction of R_{rms} with

ion fluence indicates that irradiation suppresses the maximum area peak height and maximum area valley depth. This indicates that irradiation smoothen the surface of the films. Figure 6.5 depicts the roughness histogram of the film A, B and C. It is observed that after irradiation, small change obtained in peak height gives rise to narrow peak height distribution. It has been reported by Khanam et al. (2014) that under low energy ion irradiation on TiO_2 nanoparticles having anatase phase, ions incorporated into the material brings swelling of the particles. With increasing ion fluence, excessive swelling of the particles leads to flattening and overlapping of TiO_2 nanoparticles with consequent reduction of the surface roughness. The excessively swelled particles at still higher fluence become thermodynamically unstable and split into smaller particles with smaller magnitude of surface roughness. Similar situation may prevail in the present case leading to the observed reduced surface roughness in irradiated films.

Surface topography with grain structure and 3D images of grains of film A, B and C with grain size distribution are shown in Figure 6.6 (a-c), (d-f) and (g-i), respectively. The nanostructured thin films both pristine and irradiated film show granular microstructure having distinct grain boundary. The grain size distributions are fitted to a Gaussian function. Grain analysis, demonstrates the grain size in pristine film and film irradiated at the fluence 1×10^{14} ions/cm^2 is 27.5 nm with size distribution of 20 to 70 nm, whereas after irradiating with 5×10^{16} ions/cm^2, the average grain size is decreased to 26.8 nm, showing a grain size distribution of 20 to 60 nm. It is observed that grain size distribution of film C, shifting toward smaller particle size corroborates with decrease in surface roughness. In the previous chapter, we have explained that evolution of nanoparticles under ion irradiation is expected to be governed by the confinement of a high density of energy deposited by irradiating with

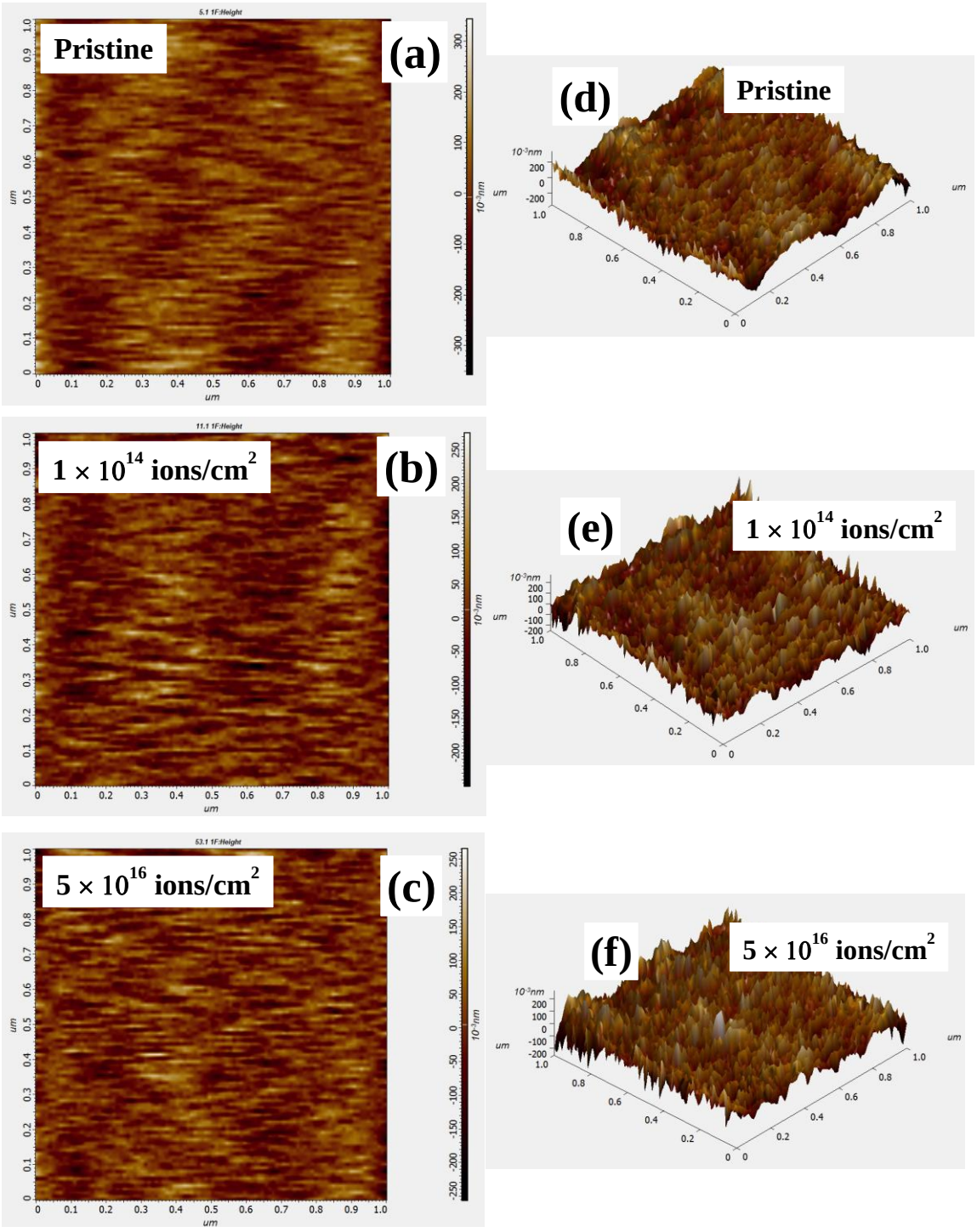

Figure 6.4 *AFM images of pristine and irradiated TiO_2 thin films A, B and C are (a), (b), (c) respectively. (d), (e) and (f) depict the 3D representation of the respective films.*

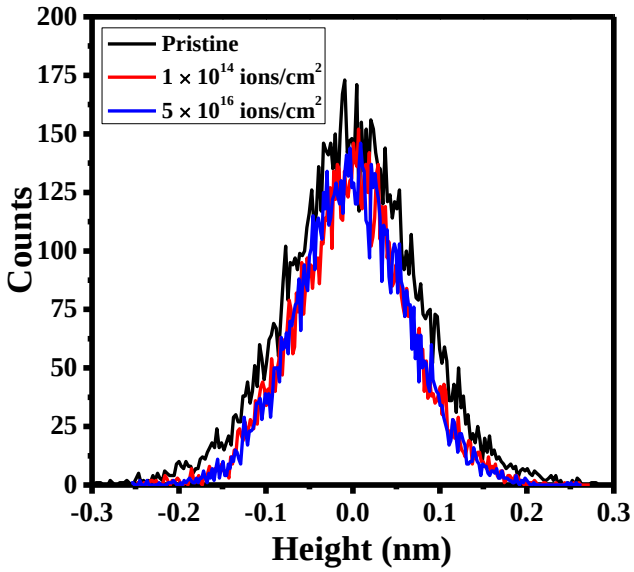

Figure 6.5 *Roughness histograms of TiO_2 thin films before and after irradiating with 500 keV Ar ion.*

500 keV ions. The energy deposited on the electrons are then transformed to the lattice by electron-phonon coupling in a time span of 10^{-4} and 10^{-12} sec which increases the lattice temperature to such a level that transient temperature rise leads to the formation of crystalline to crystalline phase transformation, as we could observe after irradiating with fluence, 5×10^{16} ions/cm^2. The heat deposited by the ions is localized and dissipates to the neighboring atom due to thermal conductivity which brings crystalline to crystalline phase transformation. Thus anatase to brookite phase transformation with intermediate amorphous phase has been observed. The presence of Ti_4O_7 however, show neither phase transformation nor amorphisation upto highest fluence indicating radiation resistant behavior.

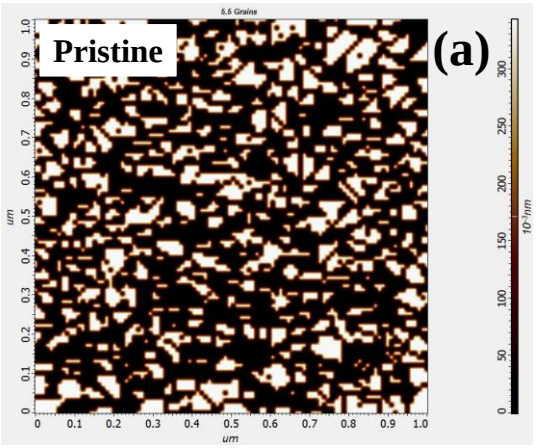
Pristine
(a)

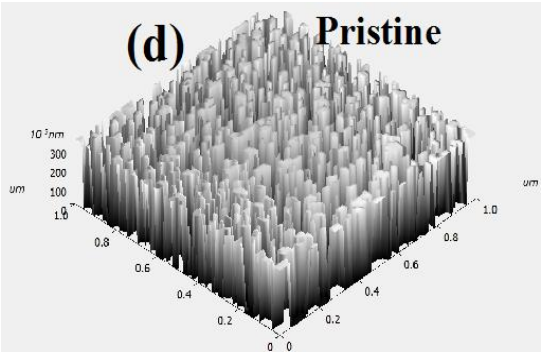
(d)
Pristine

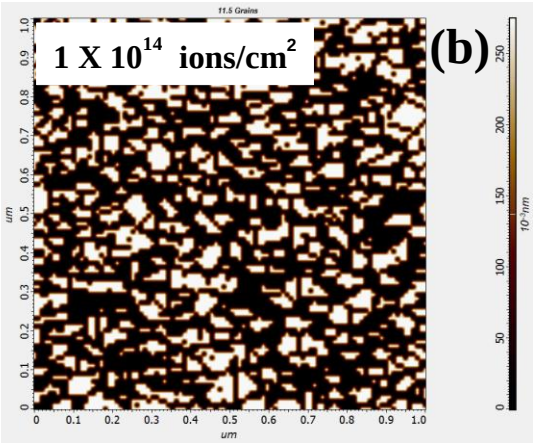
1 X 10^14 ions/cm^2
(b)

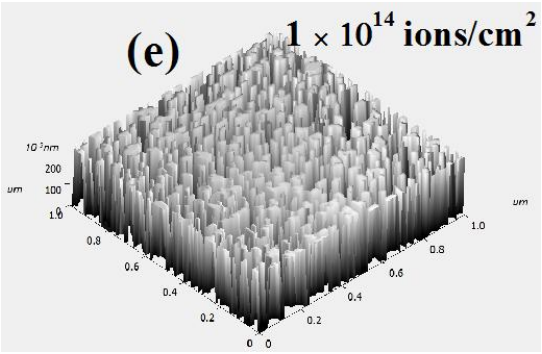
(e)
1 × 10^14 ions/cm^2

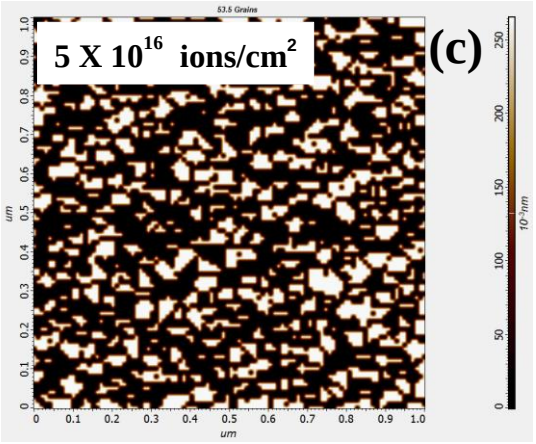
5 X 10^16 ions/cm^2
(c)

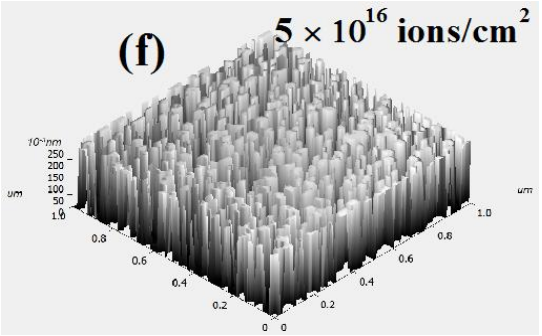
(f)
5 × 10^16 ions/cm^2

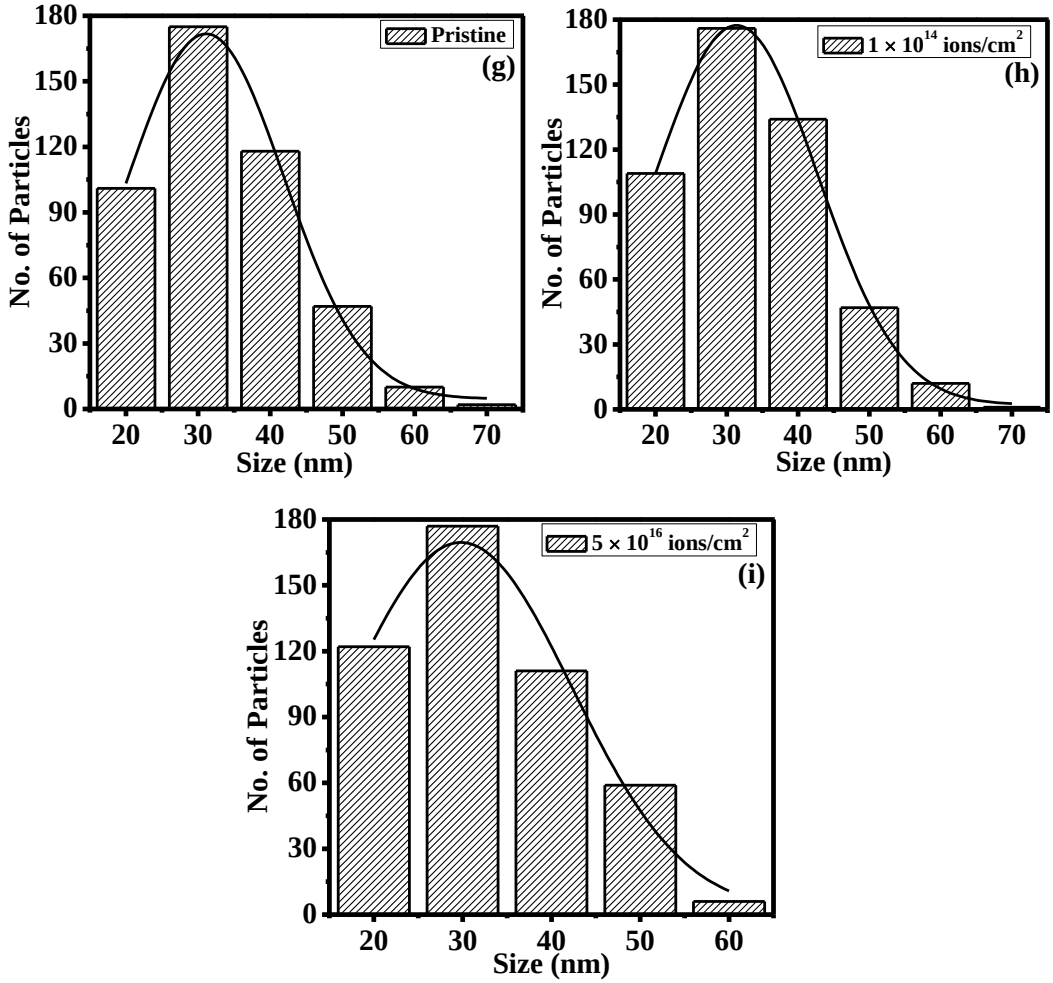

Figure 6.6 *AFM image of TiO_2 thin films with grain structure of film A, B, C are (a), (b) and (c) respectively, (d)- (f) depict the 3D representation of the respective films and (g)- (i) show grain size distribution of respective films.*

6.3 Magnetic Property

Magnetic properties have been studied in these films by carrying out field (H) dependant magntisation (M) measurement, depicted in Figure 6.7 (a). In this case the magnetic field varies from 0 to 10 kOe. The diamagnetic contribution of Si has been removed from the M vs. H data. All the films show hysteresis behavior with finite coercivity and remanence which is a signature of ferromagnetism. The zoomed view of hysteresis curves are shown in

Figure 6.7 (b). In pristine as well as in irradiated films, magnetization saturates at about 6 kOe with saturation magnetization 11.37, 7.26 and 6.27 emu/cc for film A, B and C, respectively. In case of film A and B, while corecivity is 61 Oe, remanence is found to be 1.08 and 0.45 emu/cc respectively. For film C, coercivity is 34 Oe and remanence is 0.32 emu/cc. The observation of room temperature ferromagnetism (RTFM) has been reported in

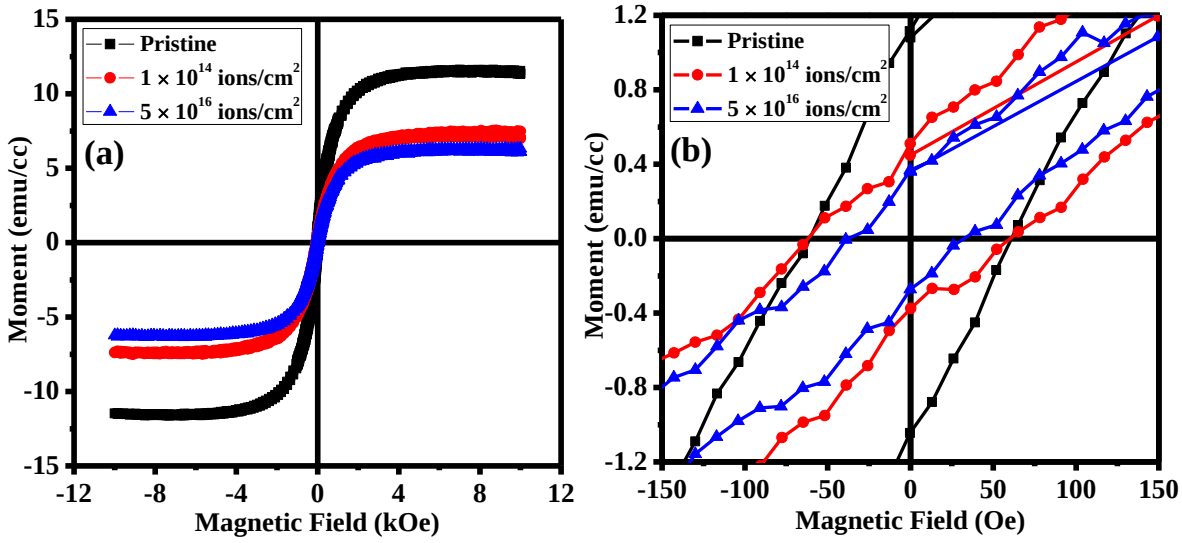

Figure 6.7 *(a) Magnetization as a function of applied magnetic field of the films, A, B, C at 300 K, (b) show the zoomed view of the M–H loops.*

TiO_2 films deposited by different techniques such as sputtering, sol–gel and PLD [Thakur et al. (2011)a and Mohanty et al. (2013, 2014)a]. However, report on RTFM demonstrated by films deposited through electron beam evaporation technique is rare. The reason behind the ferromagnetism in TiO_2 films have also been shown by many research groups. Rumaiz et al. (2007) attribute the ferromagnetism to oxygen vacancies rather than Ti^{3+}/Ti^{2+} cations. However, Wei et al. (2009) explain that 2p electron of oxygen plays an important role in the exchange interaction and ferromagnetic ordering. The presence of an oxygen vacancy is

associated with two electrons which may localize the neighboring Ti ions transforming into Ti^{3+} or may be delocalized in TiO_2 matrix. RTFM in films deposited by e-beam evaporation annealed in Ar and O_2 atmosphere has been reported earlier where the phase of the films is anatase [Mohanty et al. (2014)a]. Kim et al. (2009) have observed RTFM in both anatase and rutile phases of TiO_2. The higher magnetic moment has been attributed to more oxygen defects in the distorted TiO_6 octahedra [Thakur et al. (2011)a]. We attribute the occurrence of RTFM in all the films is due to presence of Ti_4O_7 phase where Ti is in +3 oxidation state. As Ti^{3+} is magnetic in nature, ferromagnetism would be due to the presence of Ti_4O_7. However, higher magnetization in pristine film than that of irradiated one could not be explained due to the presence of Ti_4O_7 phase only.

6.4 X-Ray Photoelectron Spectroscopy

To understand the difference in magnetization observed in pristine film (A) and in film (C), we have carried out X-ray Photoelectron Spectroscopy. Figure 6.8 (a) and (b) depict Ti 2p and O 1s core level spectra, respectively. Figure 6.8 (a) shows Ti $2p_{3/2}$ peak around the binding energy 459 eV which is at higher binding energy than that of Ti $2p_{3/2}$ of bulk phase. The difference in binding energy could be due to coexistence of TiO_2 and Ti_4O_7 phase, which is well matched with previous reports by Yao et al. (2012) and Li et al. (2010)b. O1s peak observed at 530 eV is found to be asymmetric (Figure 6.8 (b)). Fitting the asymmetric peak with two Gaussian peaks denoted as Oa and Ob, where Oa corresponds to oxygen atoms of the material and Ob is ascribed to the hydroxyl groups and organic contaminants [Bharati et al. (2018)], we observe that area under the curve Oa increases and Ob decreases after irradiation. We calculate the Ob to Oa area ratio and it is found to be 1.89

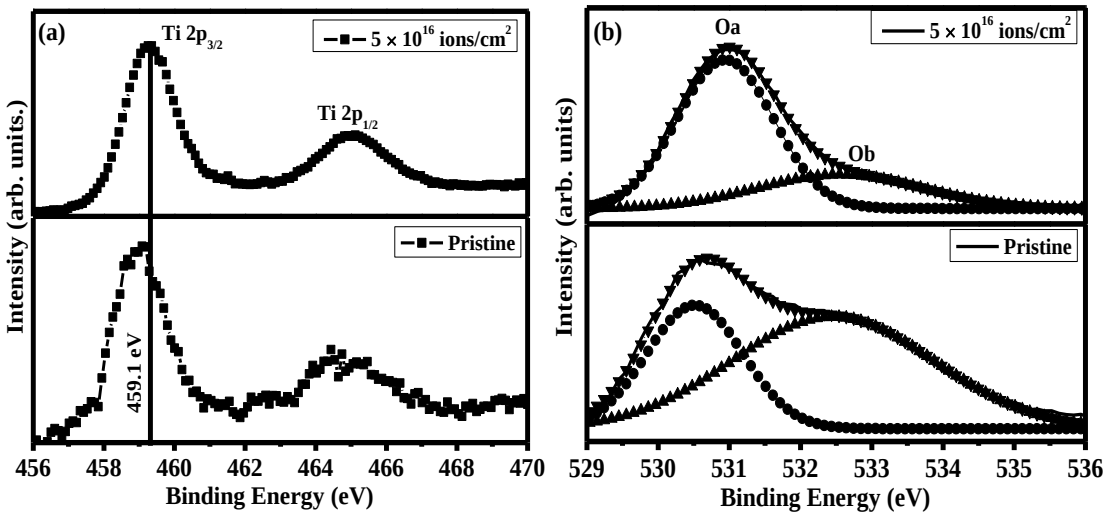

Figure 6.8 *(a) XPS of TiO_2 films A and C (a) Ti 2p core level spectra of the films A and C, (b) Oxygen 1s core level spectra of the films A and C.*

and 0.39 for film A and C, respectively. The higher Ob to Oa ratio in pristine film, A confirms the higher oxygen vacancies than the irradiated film, C. Therefore, higher magnetic moment in pristine film could be due to higher oxygen vacancies.

6.5 Conclusions

TiO_2 thin films deposited by e-beam evaporation technique and annealed at 900 ºC in O_2 environment were irradiated with 500 keV Ar^{2+} ions. Evolution of structure and magnetic properties with ion fluence in thin films were studied. From GAXRD and Raman, it was observed that pristine film crystallized in anatase phase, whereas after increasing the ion fluence to 5×10^{16} ions/cm^2, anatase to brookite phase transformation occurred with an intermediate amorphous phase at the ion fluence, 1×10^{14} ions/cm^2. The impurity phase, Ti_4O_7 observed in pristine film did not show change in the intensity of the XRD peaks after

irradiation indicated a radiation resistant behavior. No major change in film thickness before and after irradiation was evidenced from RBS measurement. From AFM, it was found that roughness was more in pristine film than in the irradiated films. Although magnetic measurements showed RTFM irrespective of phase and crystallinity, we observed abnormally high saturation magnetization in pristine films than in irradiated ones. Higher magnetization in pristine film could be due to higher oxygen vacancies, which was obtained from XPS.